Bridge-Function Pseudospectral Method for Quantum Mechanical Simulation of Nano-Scaled Devices

Yuta Saitou, Takeshi Nakamori, Satofumi Souma, and Matsuto Ogawa
Department of Electrical and Electronic Engineering, Kobe University
1-1 Rokkodai, Nada, Kobe, 657-8501, JAPAN
Email: 111t225t@stu.kobe-u.ac.jp / ogawa@eedept.kobe-u.ac.jp

***Abstract*—In this paper we show the effectiveness and powerfulness of a pseudospectral method (PSM) with newly developed bridge-functions, which ensure the continuity of physical quantities, for the solution of the 3D Schrödinger equation, Poisson's equation, in addition, non-equilibrium Green's function (NEGF) on equal footing with high accuracy and negligible computational overheads. By comparing with the results of the conventional finite difference method (FDM) with same numbers of mesh, the present method is found to be 60 times faster with higher accuracy.**

I. Introduction

Many applications of quantum mechanical phenomena in nano-scaled devices require the solutions of the Schrödinger equation, Poisson's equation, and the non-equilibrium Green's function (NEGF) which are usually performed numerically with a finite difference method (FDM) or a finite element method (FEM). However, as the dimension of the devices becomes lower, e.g. double-gate MOSFETs, gate-all-around FETs, and quantum dot devices, which are comprised of quantum wire structures or quantum dots, FDM or FEM becomes inappropriate in terms of computational costs and time. This is because the FDM/FEM, in general, requires many mesh points to achieve high accuracy. To reduce the size of the matrix and the computational time in the conventional FDM, Ren *et al*. have used a mode space technique [1]. This technique is a kind of a separation of variables method for the solution of partial differential equations, where the Schrödinger equation is solved in the plane perpendicular to the transport direction, then the subband energies and eigenfunctions are calculated. The wave function is expanded in the subbands and the resulting transport equation is simply a one-dimensional equation.

On the other hand, pseudospectral method (PSM) [2], [3] is known as an efficient numerical method alternative to FDM and FEM. Conventional PSM expands the solution in certain basis function series and computes expansion coefficients, which gives both higher accuracy and more efficient convergence. In spite of the efficiency, because of complicated form of the basis functions, it has been quite difficult to take boundary conditions into account, in particular, in the case of the problems with materials being spatially varying. We have developed a powerful method for the solution of those three equations on equal footing in order to implement efficient quantum mechanical simulations of nanodevices. In the present bridge-function pseudospectral method (BPSM), we have combined a PSM with the '*bridge functions*', which naturally guarantee the continuity of such physical quantity as probability current density and electrical flux density in adjacent intervals even when the materials under consideration are spatially varying. We have also adopted the mode space expansion technique in the present calculation.

II. Theory

Similar to the FEM, we expand any physical quantity in terms of a set of local basis functions spanning a grid of nodes $x^0\ (=0) < x^1 < x^2 < \cdots < x^I (= L)$ which replaces the independent variable x, where L is a device length and I is the total numbers of the nodal points in x direction (see Fig. 1). The present BPSM is composed of the bridge-functions, connections of two Lagrange polynomials over adjacent elements or intervals, i.e. between i and $i+1$, which are schematically illustrated in Fig. 2, and the Gauss-Lobatto (GL) quadrature [5]. The continuity of electrical flux density or probability current density, thus the electric current density is naturally guaranteed, which enables us to take the boundary conditions into account in much easier manner than the conventional PSMs.

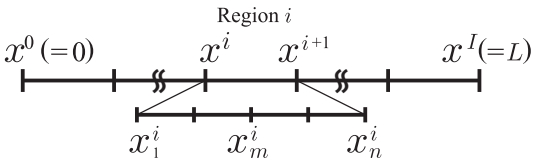

Fig. 1. The device area under consideration $[0, L]$ is divided into regions or elements in the present BPSM. I is the total numbers of the nodal points in x direction, n the numbers of local basis functions and x^i_m's the Gauss-Lobatto points, respectively.

As mentioned, in the present PSM, the region under consideration $[0, L]$ is divided into sub-regions $(i = 0, 1, \cdots, I)$ and each sub-region is spanned by a basis set: Lobbato shape functions or Lagrange interpolation polynomials $(m = 1, 2, \cdots, n)$ (see Fig. 2) [4]. The 1D orthonormal basis func-

978-1-61284-418-3/11/$26.00 © 2011 IEEE

tions are expressed as

$$\chi_{i,m}(x) = \begin{cases} \dfrac{f_{i,n}(x) + f_{i+1,1}(x)}{\sqrt{w_n^i + w_1^{i+1}}} & (m = 1) \\ \text{(Bridge function)} & \\ \dfrac{f_{i,m}(x)}{\sqrt{w_m^i}} & (m \neq 1), \end{cases} \tag{1}$$

where

$$f_{i,m}(x) = \begin{cases} \displaystyle\prod_{j \neq m} \frac{x - x_j^i}{x_m^i - x_j^i} & (x^i \leq x \leq x^{i+1}) \\ 0 & (x < x^i \ , \ x > x^{i+1}) \end{cases} \tag{2}$$

is the $(n-1)$th order Lagrange interpolation polynomial. x_m^i, w_m^i are the points and weights, respectively, in GL quadrature chosen to make Eq. (3) exact when $g(x)$ is a polynomial of degree $\leq 2n-3$:

$$\int_{x^i}^{x^{i+1}} g(x)dx \cong g(x^i)w_1^i + \left[\sum_{m=2}^{n-1} g(x_m^i)w_m^i\right] + g(x^{i+1})w_n^i. \tag{3}$$

The property that, in the GL quadrature, the integral is exact up to the order of $2n-3$ for the $(n-1)$th order polynomial guarantees higher accuracy than conventional FDM/FEM.

In conventional PSMs, the sub-region is simply expanded by orthonormal functions $\{f_m/\sqrt{w_m}\}$. One of the specific features in the present method is to use the '*bridge function*' for the solution of all three differential equations. The bridge function is comprised of the two functions $f_{i,n}$ and $f_{i+1,1}$ in the adjacent regions to guarantee continuity of physical quantity in adjacent intervals(Eq. (1) and Fig. 2 ($\chi_{1,1}$ and $\chi_{2,1}$)). By expanding the solution of each equation using these basis functions $\chi_{i,m}$, the continuity of probability current density or density of electrical flux at each interface is naturally guaranteed, which enables us to take the boundary conditions into account in much easier manner than the conventional PSMs.

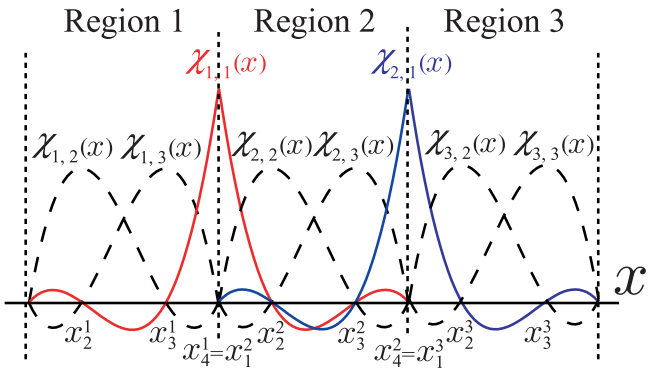

Fig. 2. 1D basis functions $\chi_{i,m}(x)$ ($I = 3$ and $n = 3$), where i indicates the region, and m the basis. The solid lines are the *bridge functions*, which ensure the continuity of any physical quantities between the adjacent regions.

In order to use the mode space expansion technique [1], we solve the 2D Schrödinger equation perpendicular to the transport direction (x). The time-independent Schrödinger equation is written as

$$\left[-\frac{\hbar^2}{2}\nabla\cdot\left(\frac{1}{m^*(\boldsymbol{r})}\nabla\right) + U\right]\psi = E\psi \tag{4}$$

where $m^*(\boldsymbol{r})$ is the spatially varying effective mass, U the hetero-junction potential, E the eigenenergy, ψ the wave function, respectively. In the 2D Schrödinger equation, the wavefunction $\psi(y,z)$ is expanded as

$$\begin{aligned}\psi(y,z) &= \sum_{i_y,m_y,i_z,m_z} c_{i_y,m_y}^{i_z,m_z}\psi(y_{m_y}^{i_y}, z_{m_z}^{i_z})\chi_{i_y,m_y}(y)\chi_{i_z,m_z}(z) \\ &\equiv \sum_{i,m} c_{i,m}\psi_{i,m}^{\mathrm{2D}}, \end{aligned} \tag{5}$$

where $c_{i,m}$ is a function of the weights, and $i = (i_y, i_z)$, $m = (m_y, m_z)$, respectively. Now, we transform the equations into the weak-form using the weight functions of weighted residual method in the FEM [6] which are same as the basis functions $\chi_{i,m}^{\mathrm{2D}} = \chi_{i_y,m_y}(y)\chi_{i_z,m_z}(z)$. The weak form of the Schrödinger equation can be represented as

$$\sum_{i,m}\left[A_{m,m'}^{i,i'\ \mathrm{2D}} + U(\boldsymbol{r}_m^i)\delta_{m,m'}\delta_{i,i'}\right]c_{i,m}\psi = Ec_{i,m}\psi, \tag{6}$$

where $\delta_{i,i'}$ and $\delta_{m,m'}$ imply Kronecker's delta, and $\boldsymbol{r}_m^i = (y_{m_y}^{i_y}, z_{m_z}^{i_z})$, respectively.

To take into account the potential distribution in the device, we have to solve the Poisson's equation self-consistently with other equations. Poisson's equation is written as

$$\nabla\cdot(\epsilon(\boldsymbol{r})\nabla)\,\varphi = -q[N_{\mathrm{D}} - n], \tag{7}$$

where $\epsilon(\boldsymbol{r})$ is the dielectric constant, which varies depending on the materials in consideration, q (> 0) the electronic charge, N_{D} the donor density, φ the electro-static potential, and n the electron concentration, respectively. In the 3D Poisson's equation, $\varphi(x,y,z)$ is expanded as

$$\varphi(x,y,z) = \sum_{i,m} c_{i,m}\varphi(x_{m_x}^{i_x}, y_{m_y}^{i_y}, z_{m_z}^{i_z})\chi_{i,m}^{\mathrm{3D}} \tag{8}$$

and the weak form can be represented as

$$\begin{aligned}&\sum_{i,m}\left[A_{m,m'}^{i,i'\ \mathrm{3D}} - \frac{q^2}{\epsilon_0 k_B T}n(\boldsymbol{r}_m^i)\delta_{m,m'}\delta_{i,i'}\right]c_{i,m}\delta\varphi \\ &= -q[N_{\mathrm{D}}(\boldsymbol{r}_m^i) - n(\boldsymbol{r}_m^i)]c_{i,m} - \sum_{i,m} A_{m,m'}^{i,i'}c_{i,m}\varphi, \end{aligned} \tag{9}$$

where $i = (i_x, i_y, i_z)$, $m = (m_x, m_y, m_z)$, $\boldsymbol{r}_m^i = (x_{m_x}^{i_x}, y_{m_y}^{i_y}, z_{m_z}^{i_z})$, and $\chi_{i,m}^{\mathrm{3D}} = \chi_{i_x,m_x}(x)\chi_{i_y,m_y}(y)\chi_{i_z,m_z}(z)$, respectively. The equation has been further transformed into a linear equation of $\delta\varphi$ which is the minimal change of the electro-static potential, since electron concentration n and the confinement potential U, equivalently φ are mutually dependent.

Since the wave function in the transverse direction is expanded in the subbands, the resulting transport equation

is simply a one-dimensional equation and drain current is calculated by NEGF. The retarded Green's function is defined as

$$\left[E+i0_+-\left\{-\frac{\hbar^2}{2}\frac{d}{dx}\left(\frac{1}{m^*(x)}\frac{d}{dx}\right)+U\right\}\right]G(x,x')=\delta(x-x'), \tag{10}$$

where $G(x,x')$ is retarded Green's function, $\delta(x-x')$ is the delta function, respectively. In the same way as mentioned previously, 1D retarded Green's function is also expanded as

$$G(x,x')=\sum_{i,m} c_{i,m}G(x')\chi_{i,m}(x) \tag{11}$$

and finally written as

$$\sum_{i,m}\left[E\delta_{i,i'}\delta_{m,m'}-A^{i,i'\ 1\mathrm{D}}_{m,m'}-\Sigma^{i,i'}_{m,m'}\right]c_{i,m}G(x^{i'}_{m'}) = \chi_{i',m'}(x^{i}_{m}), \tag{12}$$

where $\Sigma^{i,i'}_{m,m'}$ is the appropriate boundary self-energy which replace the effect of the open boundary conditions or the infinite electrodes. It can be expressed as

$$\Sigma^{i,i'}_{m,m'}=\begin{cases}-\dfrac{\hbar^2}{2m_{\mathrm{L}}}\mathrm{i}k_{\mathrm{L}} & (i=i'=1,\ m=m'=1:\text{source})\\ -\dfrac{\hbar^2}{2m_{\mathrm{R}}}\mathrm{i}k_{\mathrm{R}} & (i=i'=I,\ m=m'=n:\text{drain})\\ 0 & (\text{other}),\end{cases} \tag{13}$$

where i is the imaginary unit and $k_{\mathrm{L/R}}$ is wavenumber of the electron at source or drain electrode, respectively.

The matrix element $A^{i,i'\ 3\mathrm{D}}_{m,m'}$ in Eq. (9) is written as

$$A^{i,i'\ 3\mathrm{D}}_{m,m'}=(\delta_{i,i'}+\delta_{i,i'\pm1^*})\times \int_R\left(\frac{\partial\chi_{i',m'}}{\partial x}\eta\frac{\partial\chi_{i,m}}{\partial x}+\frac{\partial\chi_{i',m'}}{\partial y}\eta\frac{\partial\chi_{i,m}}{\partial y}+\frac{\partial\chi_{i',m'}}{\partial z}\eta\frac{\partial\chi_{i,m}}{\partial z}\right)d\boldsymbol{r} \tag{14}$$

with the Kronecker's delta representing the fact that bridge function is only beyond adjacent intervals, $i'\pm1^*=(i'_x\pm1,i'_y,i'_z)$ or $(i'_x,i'_y\pm1,i'_z)$ or $(i'_x,i'_y,i'_z\pm1)$. $A^{i,i'\ 2\mathrm{D}}_{m,m'}$ in Eq. (6) and $A^{i,i'\ 1\mathrm{D}}_{m,m'}$ in Eq. (12) are written similarly. η equals $1/m^*$ in the Schrödinger equation and NEGF or ϵ in the Poisson's equation, respectively.

The integration of Eq. (14) is evaluated by the GL quadrature which ensures the higher accuracy. For example, the first term of the integration in Eq. (14) is evaluated as

$$\begin{aligned}A_{\partial x}&=\iiint\chi'_{i'_x,m'_x}\chi_{i'_y,m'_y}\chi_{i'_z,m'_z}\chi'_{i_x,m_x}\chi_{i_y,m_y}\chi_{j_z,n_z}\,dxdydz\\ &\simeq\delta_{i_y,i'_y}\delta_{m_y,m'_y}\delta_{i_z,i'_z}\delta_{m_z,m'_z}\\ &\quad\times\sum_{i_x,m_x}w^{i_x}_{m_x}\chi'_{i'_x,m'_x}(x^{i_x}_{m_x})\chi'_{i_x,m_x}(x^{i_x}_{m_x}),\end{aligned} \tag{15}$$

where $\chi'=d\chi(x)/dx$. Other terms can be similarly evaluated.

III. Result and Discussion

In order to show the superiority of the present method in terms of accuracy and computational costs over conventional FDM, we have applied the BPSM to the analysis of I-V characteristics of a gate-all-around Si nano-wire MOSFET (SiNW FET)(Fig. 3) [7], where Schrödinger-Poisson equations and NEGF are solved simultaneously and self-consistently. The orientation dependent effective masses in the conduction band of Si [8] are also taken into account in the calculation.

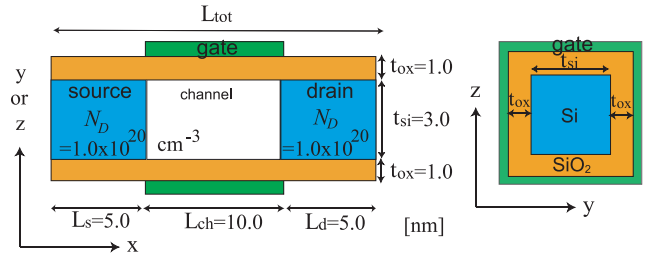

Fig. 3. Model structure of a SiNW FET [7] under investigation. The channel orientation is along ⟨100⟩.

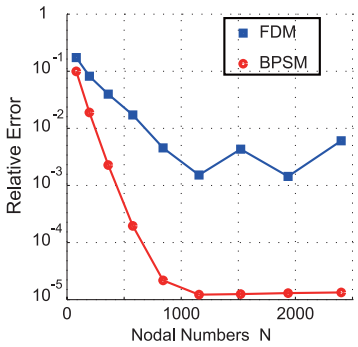

Fig. 4. Comparison of the relative errors of the first eigenstate between FDM and BPSM as a function of total nodal numbers N.

Figure 4 shows the comparison of the errors of the first eigenenergy obtained in both the FDM and BPSM as a function of entire nodal numbers N in the self-consistent Schrödinger-Poisson calculations in the cross-section of the SiNW FET. It should be noted that accuracy of calculated result by the BPSM is much higher than that of the FDM when N is comparable, in addition, the refinement rate of accuracy with increase of N is much faster.

Figure 5 shows the comparison of the first subband profile along the channel calculated by the FDM (solid lines, with longitudinal nodal number $N_x=32$) with increasing the cross-sectional nodal number N_{yz} to that calculated by the BPSM (dotted line, with $N_x=32$ and $N_{yz}=400$ which are checked to give enough accurate results). It is important to notice that although the result of the FDM approaches that of the BPSM as N_{yz} increases, there still exist errors between them, which can be understood from Fig. 4, that is, poorer convergence of the FDM in the transverse direction has resulted in the

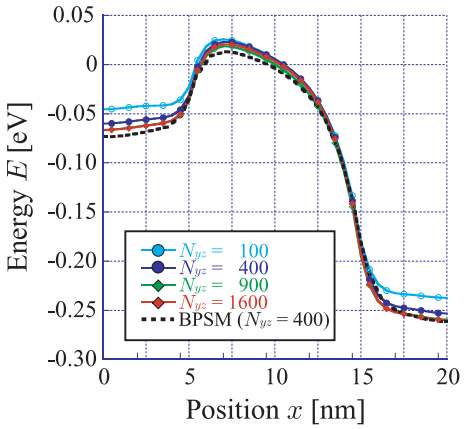

Fig. 5. First subband profile along the channel at $V_{\rm d} = 0.2\ V$ and $V_{\rm g} = 0.4\ V$, where the dotted line is obtained by the BPSM with $N_{yz} = 400$, while solid lines are, for comparison, by the FDM increasing the cross-sectional nodal number N_{yz} with the nodal numbers (N_x) fixed in the transport direction.

significant difference in the subband profile even though finer mesh is adopted.

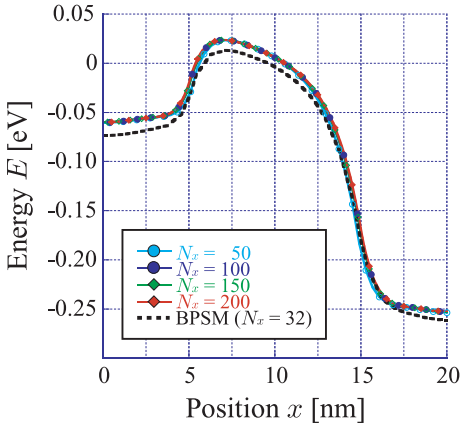

Fig. 6. First subband profile along the channel, where the dotted line is obtained by the BPSM with $N_x = 32$, while solid lines are for comparison by the FDM increasing the cross-sectional nodal number N_x with N_{yz} fixed.

Figure 6 also shows the comparison of the first subband profile by the FDM with increasing N_x to the BPSM (dotted line). As seen in these figures, the subband profile is more sensitive to N_{yz} than to N_x. This is because the eigenenergies in the cross-sectional area (transverse direction) are sensitive to the confinement potential or the carrier concentration distribution and the eigenenergy calculation by the FDM shows the poorer results as shown in Fig. 4.

Figure 7 compares the $I_{\rm d}$-$V_{\rm g}$ characteristics between FDM and BPSM when the nodal numbers are same ($N_x = 32$ and $N_{yz} = 400$). The results show that there is a large difference in the calculated drain current amounting as much as 18 %, which may mislead to incorrect estimation of $V_{\rm th}$. The large discrepancy arises from the fact, as can be understood from Figs.4-6, that the FDM gives inaccurate eigenvalues in each cross-section or inaccurate subband profiles along the channel while the present BPSM gives more accurate results.

As far as the CPU time is concerned in the self-consistent calculation on an Intel Xeon (2.3GHz) processor, the present BPSM is found to show 60 times faster than the conventional FDM. This is because the present BPSM requires fewer nodal points than the FDM to attain desirable accuracy, specifically in the eigenvalue calculation in the transverse direction.

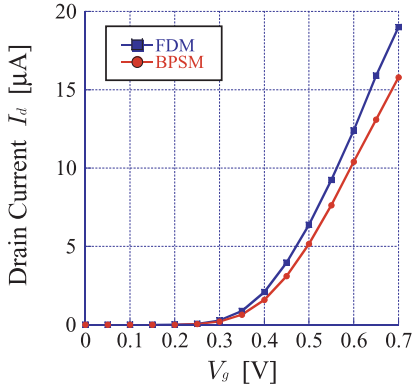

Fig. 7. Comparison of the $I_{\rm d}$-$V_{\rm g}$ characteristics between FDM and BPSM when the entire nodal numbers are same in each method.

IV. Conclusion

We have presented the superiority of the proposed BPSM over the conventional FDM. The capability of the present method is essentially due to the implementation of the bridge-functions into a conventional PSM with the Gauss-Lobatto quadrature which preserves the computational accuracy and continuity of physical quantities, thus preventing complexity of matrix elements and convergence issues. Further refinement in accuracy of the calculation and reduction of computational costs can be achieved by the usage of an adaptive mesh generation. Since Schrödinger equation, Poisson's equation, and NEGF are commonly used and quite versatile for quantum mechanical device simulation, the capability of the present BPSM can be universally applied not only to the SiNW FET model but also to any other quantum mechanical device simulations.

References

[1] Z. Ren, R. Venugopal, S. Goasguen, S. Datta, and M.S. Lundstrom, IEEE Trans. Electron Devices, **50** 1914 (2003).
[2] J. C. Light, I. P. Hamilton, and J. V. Lill, J. Chem. Phys. **82**, 1400 (1985).
[3] D.E. Manolopoulos and R.E. Wyatt, Chem. Phys. Lett. **152**, 23 (1988).
[4] T.N. Rescigno, and C.W. McCurdy, Phys. Rev. A **62**, 032706 (2000).
[5] G.H. Golub and J.H. Welsch, Mathematics of Computation **23** (106), 221 (1969).
[6] L. Ramdas Ram-Mohan, *Finite Element and Boundary Element Applications in Quantum Mechanics*, Oxford (2002).
[7] S. Bangsaruntip, A. Majumdar, and J.W. Sleight, 2010 Symposium on VLSI Technology Digest, 21 (2010).
[8] S.M. Sze and Kwok K. Ng, *Physics of Semiconductor Devices*, 3rd ed., Chap. 1, John Wiley & Sons (2007).